

Large Seebeck coefficient driven by “pudding mold” flat band in hole-doped CuRhO_2

Amitayush Jha Thakur,^{1,2} Maximilian Thees,¹ Franck Fortuna,¹
Emmanouil Frantzeskakis,¹ Daisuke Shiga,^{3,4} Hiromichi Kuriyama,⁵ Minoru Nohara,⁶
Hidenori Takagi,^{7,8} Hiroshi Kumigashira,^{3,4} and Andrés F. Santander-Syro^{1,*}

¹*Université Paris-Saclay, CNRS, Institut des Sciences Moléculaires d’Orsay, 91405, Orsay, France*

²*Donostia International Physics Center, 20018 Donostia-San Sebastián, Spain*

³*Institute of Multidisciplinary Research for Advanced Materials (IMRAM), Tohoku University, Sendai, 980-8577, Japan*

⁴*Photon Factory, Institute of Materials Structure Science,*

High Energy Accelerator Research Organization (KEK), 1-1 Oho, Tsukuba 305-0801, Japan

⁵*Department of Advanced Materials Science, The University of Tokyo, Kashiwa 277-8561, Japan*

⁶*Department of Quantum Matter, Hiroshima University, Higashi-Hiroshima 739-8530, Japan*

⁷*Department of Physics, The University of Tokyo, Tokyo 113-0033, Japan*

⁸*Max Planck Institute for Solid State Research, 70569 Stuttgart, Germany*

We report the measurement, using angle-resolved photoemission spectroscopy, of the metallic electronic structure of the hole-doped thermoelectric oxide $\text{CuRh}_{0.9}\text{Mg}_{0.1}\text{O}_2$. The material is found to have a “pudding mold” type band structure, with a nearly flat band edge located near the Fermi level, which is thought to be the origin of the thermoelectric behavior of this material. The experimental data match the density functional theory of the undoped parent compound, simply corrected by a rigid shift of the bands. Transport calculations based on the observed band structure yield a Seebeck coefficient of $\sim 200 \mu\text{V}/\text{K}$ for the undoped parent material, consistent with experimental measurements. Our results show that CuRhO_2 is a textbook example of how pure band-structural effects can result in a large thermoelectric figure of merit, demonstrating that flat band edges in oxides are a realistic route for the efficient conversion of thermal energy.

INTRODUCTION

Materials that can efficiently convert thermal energy into electricity and vice versa, i.e. good thermoelectric materials, are desirable for solid-state cooling applications and waste heat conversion to usable energy [1]. Among many classes of materials under consideration for thermoelectric device applications, such as bismuth chalcogenides [2] or lead telluride [3], oxides possess the advantages of thermal stability (hence operability at high temperatures), low toxicity and high oxidation resistance [4].

The thermoelectric performance of a material is characterized by the thermoelectric figure of merit $ZT = S^2\sigma T/\kappa$, where S is the Seebeck coefficient, σ is the electrical conductivity, T is the temperature, and κ is the thermal conductivity. A high Seebeck coefficient, along with good electrical conductivity and low thermal conductivity, is therefore critical for potential applications. However, materials with large carrier concentration, and hence a good electrical conductivity like most metals, usually have a low Seebeck coefficient and large thermal conductivity [5]. Doping to introduce carriers increases both the electrical and electronic thermal conductivity, due to the Wiedemann-Franz law [6], so this strategy to increase the figure of merit requires efforts to reduce the lattice thermal conductivity.

Recent theoretical works have shown that materials with a nearly flat band within $k_B T$ of Fermi level (μ) have both a large Seebeck coefficient and an increased electronic conductivity, suggesting an alternative route

to achieve a large figure of merit. As demonstrated in [7], under the reasonable assumption that the quasiparticle lifetime $\tau(\mathbf{k})$ is momentum-independent, and considering only the diagonal part of the Seebeck coefficient tensor as S , one can approximately write

$$S = \frac{k_B \sum_{\mathbf{k}}' v_B^2 - v_A^2}{e \sum_{\mathbf{k}}' v_B^2 + v_A^2}, \quad (1)$$

where k_B is the Boltzmann constant, $e < 0$ is the electron charge, $\varepsilon(\mathbf{k})$ is the momentum-dependent energy of the conduction band, $\sum_{\mathbf{k}}'$ is a sum over \mathbf{k} states with $|\varepsilon(\mathbf{k}) - \mu| < k_B T$, and v_A, v_B are respectively the group velocities of states just above and below the chemical potential μ . The presence of a flat band just above (below) μ which changes to a highly dispersive band below (above) μ , i.e. $v_A^2 \ll v_B^2$ ($v_A^2 \gg v_B^2$), results in a large value of $|S| \sim O(k_B/|e|) \sim O(100)\mu\text{V}/\text{K}$ along with relatively low resistivity coming from the conducting band, which results in a strong enhancement in the thermoelectric figure of merit ZT . This type of band structure is referred to as the “pudding mold” type band, and has been theoretically investigated in oxides such as Na_xCoO_2 [7], LaRhO_3 and CuRhO_2 [8] and other materials like FeAs_2 and PtSe_2 [9].

Transition-metal oxides, some of which are both conductive and thermoelectric materials, are in principle good candidates for realizing such “pudding mold” band scenario, thanks to the narrow d -orbitals constituting their conduction band and the natural occurrence of layered structure which promotes in-plane electrical conductivity and minimizes the out-of-plane thermal conductivity

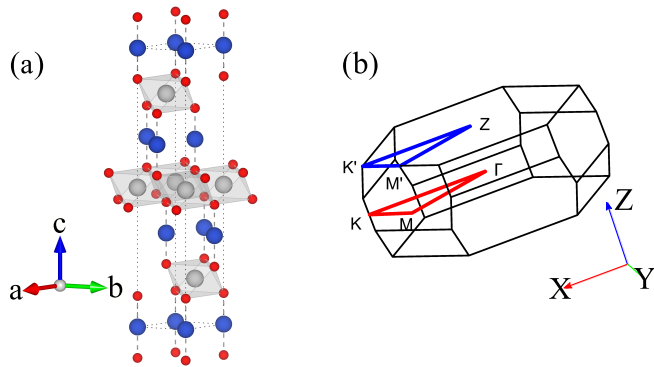


Figure 1. (a) The conventional hexagonal unit cell of CuRhO_2 , with atoms colored red (O), blue (Cu), and gray (Rh). (b) Brillouin zone (BZ) of CuRhO_2 , showing high-symmetry points (Γ , K , M) and the path used for band structure calculations.

ity [10]. In particular, the layered oxide CuRhO_2 has raised interest as thermoelectric material [8, 11, 12]. It belongs to the 166 – $R\bar{3}m$ space group with the typical delafossite structure, with RhO_2 layers stacked between the triangular Cu layers (see Fig. 1), a semiconducting band gap of 1.9 eV [13], and a high Seebeck coefficient of $\sim 200 \mu\text{V}/\text{K}$ at 300 K [12]. Mg substitution of Rh sites leads to the introduction of hole carriers in the material, resulting in a transition to a metallic state. The Seebeck coefficient decreases systematically with doping in single-crystalline samples, but the 10% Mg-substituted compound $\text{CuRh}_{0.9}\text{Mg}_{0.1}\text{O}_2$ (CRMO) still exhibits a relatively large Seebeck coefficient of $\sim 100 \mu\text{V}/\text{K}$ at 300 K [12].

On the other hand, as narrow d -bands might also result in strong electron correlations, another mechanism for the enhancement of the Seebeck coefficient has been proposed in transition-metal oxides, namely correlation-induced spin degeneracy, as demonstrated e.g. in the case of NaCo_2O_4 [14]. Therefore, accessing the experimental electronic structure of thermoelectric transition-metal oxides is essential to disentangle the effects of strong correlations from those of pure band-structural origin, and to verify the mechanism driving the enhanced Seebeck coefficient. More generally, an experimental demonstration of a “pudding mold” band in a good thermoelectric material, together with a proof that such band structure is at the origin of the material’s large Seebeck coefficient, has been so-far missing.

In this paper we report the direct observation, through angle-resolved photoemission spectroscopy (ARPES), of a “pudding mold” electronic structure of metallic 10% Mg doped CuRhO_2 (CRMO). We compare our results with density functional theory (DFT) calculations, which confirm the presence of a nearly flat band edge near the Fermi level and yield a theoretical estimate of the See-

beck coefficient that agrees well with the experimental measurements.

Single crystals of $\text{CuRh}_{0.9}\text{Mg}_{0.1}\text{O}_2$ were synthesized using the self-flux method. First, polycrystalline samples were prepared by reacting a stoichiometric mixture of CuO , Rh_2O_3 , and MgO at 1050 °C for 24 hours with intermediate grinding. The resulting powder was then mixed with CuO at a ratio of $\text{CuO}:\text{CuRh}_{0.9}\text{Mg}_{0.1}\text{O}_2 = 10:1$ in a platinum crucible. The mixture was heated to 1200 °C for 5 hours, then slowly cooled to 1050 °C at a rate of 0.5 °C per hour, followed by rapid cooling to room temperature at a rate of 300 °C per hour. Finally, the residual flux was removed using an aqueous solution of 1 M HNO_3 .

ARPES measurements were performed using synchrotron radiation at the BL2-A (Mushashi) beamline in Photon Factory, KEK. The electron analyzer in the setup was Scienta-Omicron SES-2002. Soft X-rays (SX) photons with linear horizontal (LH) polarization—that is, p-polarized with respect to the measurement geometry—in the energy range of 500–620 eV, and vacuum ultraviolet (V-UV) photons at 182 eV with LH polarization were used. The CRMO samples were cleaved along [001] and measured in UHV conditions with pressure maintained around 5×10^{-11} mbar at a temperature of 20 K. The Fermi level was set by fitting a Fermi function convoluted with a linear function to the momentum integrated energy slices of the energy-momentum measurements.

DFT calculations of CuRhO_2 electronic structure were performed with the QUANTUM ESPRESSO [15] code with a plane wave basis, using a polarized general gradient approximation (GGA) exchange-correlation functional of Perdew-Burke-Ernzerhof (PBE) from the Standard solid-state pseudopotentials (SSSP) efficiency library [16, 17]. The plane wave kinetic energy cutoff is set to 55 Ry and the charge density kinetic energy cutoff is 440 Ry.

To simulate 10% Mg-doped CuRhO_2 , we performed electronic structure calculations on undoped CuRhO_2 with a small modification to its crystal structure. The lattice parameters were set to $a = 3.068 \text{ \AA}$ and $c = 17.09 \text{ \AA}$ (with respect to the conventional hexagonal lattice). To simulate the doped material, the lattice parameter a was set to be approximately 0.2% smaller than the value reported for undoped CuRhO_2 in Ref. [18]. This adjustment accounts for the reduction in the average ionic radius at the Rh site due to Mg doping, as described in Ref. [12]. The parameter c remains the same as that for the undoped material. The unit cell was then relaxed by allowing the atomic positions to adjust while keeping the cell dimensions fixed. Finally, the calculated bands were aligned with the band measured in the Mg-doped compound by applying a rigid band shift of -0.06 eV from the top of the valence band maximum. This shift provides a first approximation of the electronic structure changes induced by hole doping via Mg substitution. The value

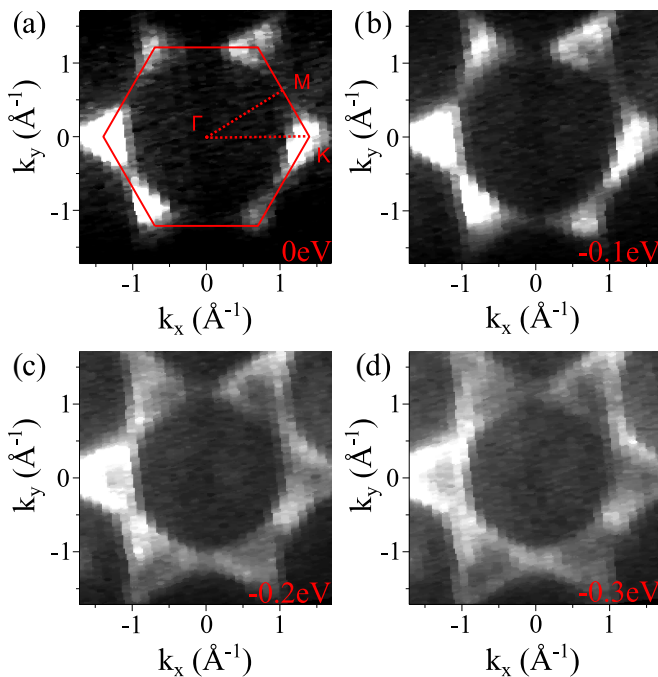


Figure 2. Constant energy maps of CuRhO₂ measured at $h\nu = 182$ eV (Maps at SX energy of $h\nu = 542$ eV are presented in Supplementary Material, Section S4). Maps are shown at energies of (a) 0 eV, (b) -0.1 eV, (c) -0.3 eV, and (d) -0.4 eV relative to the Fermi level. The hexagonal BZ is overlaid in red in (a).

of 0.06 eV was determined by observing the shift in the Fermi level in the DOS obtained from a supercell (SC) calculation consisting of 10 Rh sites, in which one Rh atom was replaced by a Mg atom that corresponds to 10% Mg doping (Supplementary Material, Section S1).

The BoltzTrap package [19] utilizing semi-classical transport equations was used to calculate the Seebeck coefficient based on the DFT band structure of the doped material. The calculation of Seebeck coefficient of the undoped material was also done for comparison, based on the DFT calculations of pristine CuRhO₂ structure ($a = 3.075$ Å and $c = 17.09$ Å) without any band shifts.

As shown in Fig. 2(a), the Fermi surface of CRMO at the bulk Γ plane is composed of six symmetrical triangular hole-like pockets centered at the high-symmetry K -points. Figs. 2(b-d) show the evolution of the constant energy surface at different energies.

Fig. 3(a) shows the second derivative intensity plots of the ARPES dispersion, calculated along the energy axis. The ARPES data, measured along the high-symmetry paths $K-M-\Gamma-K$ at 542 eV and $K'-M'-Z-K'$ at 590 eV, are overlaid with the corresponding DFT calculations. For reference, the unprocessed (raw) ARPES dispersions can be found in Section S3 of the Supplementary Material. Fig. 3(b) shows the out-of-plane Fermi surface map, spanning the Γ_{11} (referring to $\Gamma_{<0011>}$) and Z_{11} (referring to $Z_{<0011>}$) high symmetry points in reciprocal space. The corresponding ARPES energy-momentum

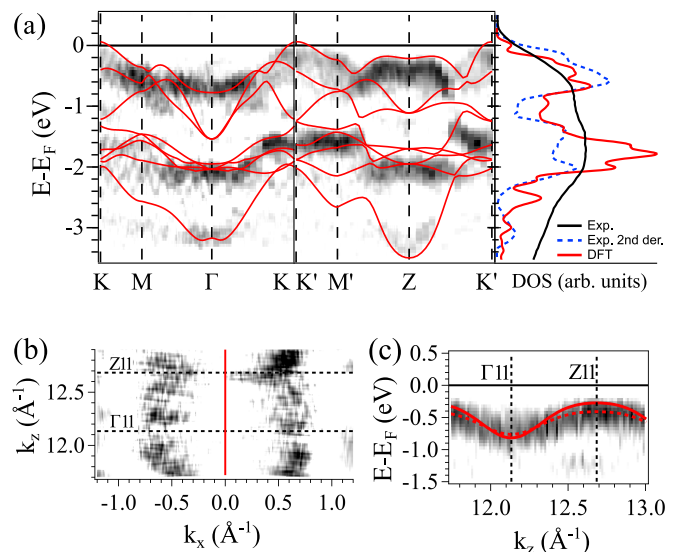


Figure 3. (a) Left: ARPES in-plane band dispersion along $K-M-\Gamma-K$ at 542 eV and $K'-M'-Z-K'$ at 590 eV. Right: Angle-integrated energy dispersion for raw ARPES data (black curves), second derivative intensity (dashed blue curves) and calculated DOS (red curves). (b) Out-of-plane Fermi surface along $k_z - k_x$ plane, spanning the high symmetry points Γ_{11} ($h\nu = 538$ eV) and Z_{11} ($h\nu = 590$ eV). (c) Energy-momentum dispersion along k_z (normal emission) with k_x along $M-\Gamma-M$ direction. Red solid curves represent theoretical bands, while dotted red curves show experimental fits. In panels (b) and (c), the data was obtained using photons in the range of 500 – 620 eV energy. Γ_{11} is calculated to lie at 538 eV by fitting with the k_z measurement and using an inner potential of 23.5 eV in the three step model approximation [20].

dispersion along k_z (momenta along out-of-plane z direction), shown in Fig. 3(c), reveals a cosine-like band dispersion with an electron-like minimum around $k_z = \Gamma$ and a hole-like maximum at $k_z = Z$. The experimental bandwidth along k_z is smaller than the calculated one by a factor of about 0.65. This can be due to unaccounted correlations of the Rh 4d t_{2g} orbitals in the calculations. This discrepancy in band dispersion along k_z is also seen in the in-plane dispersion at $k_z = Z$ (Fig. 3(a)), where the valence band maxima around Z is shifted ~ -0.2 eV compared to the calculations.

We also compare the calculated DOS with the angle-integrated ARPES intensity in Fig. 3(a). The raw angle-integrated intensity exhibits broad peaks centered around -0.7 eV and -1.7 eV that align with the main features of the calculated DOS, but it does not capture the finer peak structures or the precise bandwidths. In contrast, the angle-integrated intensity of the second derivative resolves the finer double-peak feature near the Fermi level, as well as the bandwidths of the bands around -0.7 eV and -1.7 eV. From the ARPES measurements of the dispersion and the angle-integrated intensities, the conduction band bandwidth is determined to be ~ 0.8 eV, which matches the calculations. Overall, the DFT calculations accurately reproduce the experimentally observed elec-

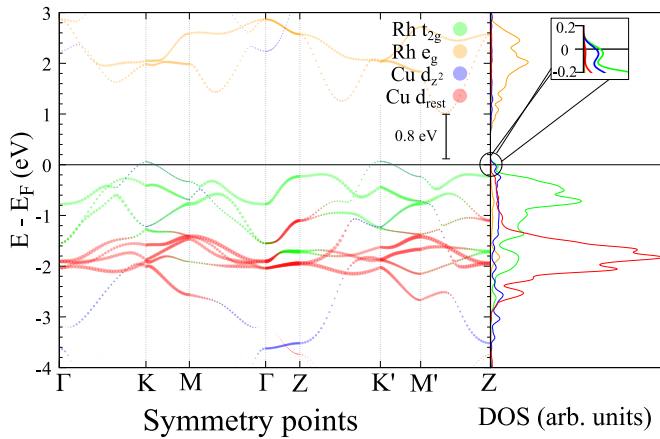


Figure 4. Left: Orbital-projected bands of CRMO (with the Fermi level set shifted to -0.06 eV from the top of the valence band) with orbital weights indicated by the size of coloured circles. Right: Orbital-projected DOS. Inset: A closer view of the DOS near the Fermi level shows the density of Rh t_{2g} orbitals and Cu d_{z^2} orbitals are similar at the Fermi level. Cu d_{rest} refers to the combined weight of the Cu d orbitals excluding the Cu d_{z^2} orbital. Vertical black line indicates gap between conduction band minima and valence band maxima.

tronic structure.

As shown in Fig. 4, the calculated gap between the valence band maxima and the conduction band minima is ~ 0.8 eV, which is smaller than the experimental value of ~ 1.9 eV for the undoped material. This discrepancy can be attributed to the underestimation of the insulating band gap by DFT [21]. Although DFT+U calculations match the experimental gap more closely, the overall dispersion from standard DFT is in closer agreement with experimental band structure data (see Supplementary Material, Section S2). The calculations indicate that the conduction band edge of CRMO exhibits distinct orbital characters depending on momentum. At the K and K' points, the conduction band comprises Cu $3d_{z^2}$ states hybridized with Rh $4d t_{2g}$ orbitals, whereas at the Γ and Z points it is composed entirely of Rh t_{2g} orbitals.

From the calculated bands, the in-plane group velocities near K (i.e. top of the conduction band) are $v_A = 0.57$ eV \AA and $v_B = 1.00$ eV \AA , while the group velocities near K' are $v_A = 0.49$ eV \AA and $v_B = 1.36$ eV \AA averaged within an energy window of $k_B T \approx 1000$ K around the Fermi level. Assuming that the in-plane Seebeck coefficient in CRMO comes essentially from electronic states around K' , and using the above values of group velocities above and below E_F around K' , one obtains from Eq. 1, an estimated value of $S \sim 66$ $\mu\text{V}/\text{K}$ which is of the same order as the experimental value of ~ 100 $\mu\text{V}/\text{K}$ in CRMO measured at 300 K [12].

To better illustrate the “pudding mold” nature of the bands, the in-plane bands along Γ - K - M - Γ and the out-of-plane bands along Γ - K - K' - Z for CRMO are plotted in Fig. 5. For the in-plane bands, we observe that the con-

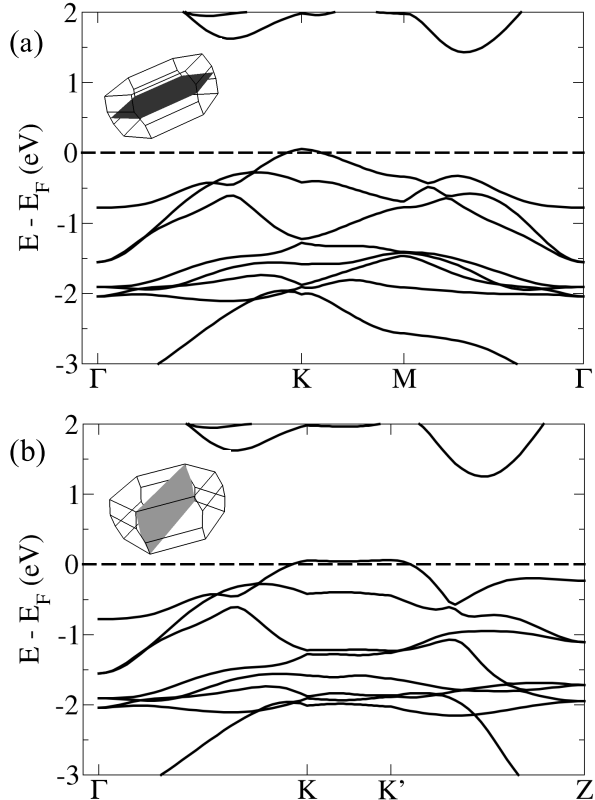


Figure 5. Band structure plots along (a) Γ - K - M - Γ and (b) Γ - K - K' - Z high-symmetry points. The plane in which these high-symmetry points lie, located within the Brillouin zone, is illustrated in the inset.

duction band maximum lies just above the Fermi level at the K point. This feature results in an enhancement of the Seebeck coefficient as $v_A < v_B$ in the small region around K . However, the out-of-plane conduction band has a large flat region between the K and K' points and is a model example of the “pudding mold” band structure. This “pudding mold” feature leads to a greater enhancement of the Seebeck coefficient in the out-of-plane direction.

Fig. 6 shows the calculated Seebeck coefficients for the undoped and the 10% doped material. Undoped CuRhO_2 has a Seebeck coefficient of ~ 200 $\mu\text{V}/\text{K}$ at 300 K, and the 10% doped sample CRMO has a Seebeck coefficient of ~ 70 $\mu\text{V}/\text{K}$ at 300 K. These values closely match the values measured for polycrystalline samples [22]. However, they are slightly smaller than the values measured for single crystals [12]. This discrepancy might be due to the effects of electron-phonon interactions observed in CuRhO_2 single crystals [12]. Furthermore, the comparisons between the in-plane (S_{xx}) and out-of-plane (S_{zz}) Seebeck coefficient show that, above 300 K, the out-of-plane component of the Seebeck coefficient increases faster than the in-plane component. This is ascribed to the flatter dispersion in the K - K' direction. The high

value of $S_{zz} \sim 256 \mu\text{V}/\text{K}$ at 1000 K for the doped sample is very close to the experimental value of $\sim 260 \mu\text{V}/\text{K}$ reported in Ref. [11].

In conclusion, our ARPES observations of the electronic structure near the Fermi level for CRMO fit well with the calculated band structure and its description in terms of the “pudding mold” band model. Our work provides an experimental basis for the realization of materials with large Seebeck coefficients and thermoelectric figure of merit, originating from a flat conduction band with the band edge lying close to the Fermi level.

ACKNOWLEDGEMENTS

Work at ISMO was supported by public grants from the Agence Nationale de la Recherche (ANR), project Fermi-NESt No. ANR-16-CE92-0018, by the “Laboratoire d’Excellence Physique Atomes Lumière Matière” (LabEx PALM) projects ELECTROX, 2DEG2USE and 2DTROX, overseen by the ANR as part of the “Investissements d’Avenir” program ANR-10-LABX-0039, and by the CNRS International Research Project EXCELSIOR. Work at Tohoku University was supported by Grants-in-Aid for Scientific Research (Nos. 16H02115 and 16KK0107) from the Japan Society for the Promotion of Science. Experiments at KEK-PF were performed under the approval of the Program Advisory Committee (Proposals 2016G621 and 2018S2-004) at the Institute of Materials Structure Science at KEK. This work was performed using HPC resources from the Mésocentre computing center of CentraleSupélec and École Normale Supérieure Paris-Saclay supported by CNRS and Région Île-de-France (<http://mesocentre.centralesupelec.fr/>).

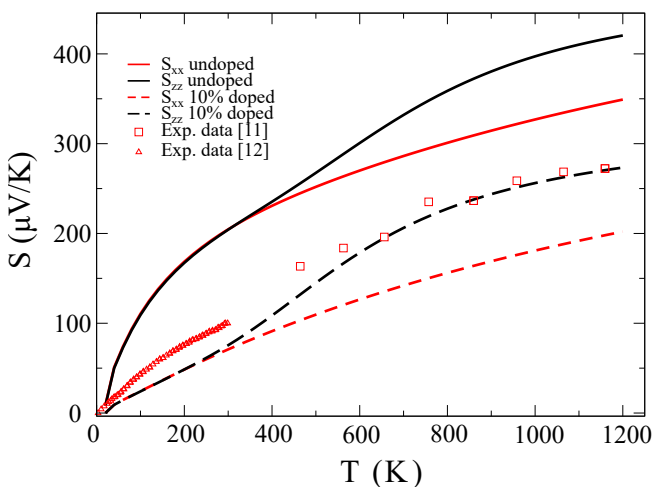


Figure 6. The S_{xx} and S_{zz} components of the calculated Seebeck coefficient versus temperature level for the undoped sample and the 10% doped sample. Experimental data from [11] and [12] are compared to the calculations of the doped Seebeck coefficient.

* andres.santander-syro@universite-paris-saclay.fr

- [1] G. D. Mahan and J. O. Sofo, The best thermoelectric., *Proceedings of the National Academy of Sciences* **93**, 7436 (1996).
- [2] I. T. Witting, T. C. Chasapis, F. Ricci, M. Peters, N. A. Heinz, G. Hautier, and G. J. Snyder, The Thermoelectric Properties of Bismuth Telluride, *Advanced Electronic Materials* **5**, 1800904 (2019).
- [3] A. D. LaLonde, Y. Pei, H. Wang, and G. Jeffrey Snyder, Lead telluride alloy thermoelectrics, *Materials Today* **14**, 526 (2011).
- [4] Y. S. Malakhov and G. V. Samsonov, Regularities governing the thermal stability of oxides of the transition metals, *Soviet Powder Metallurgy and Metal Ceramics* **5**, 981–986 (1966).
- [5] F. J. Blatt, P. A. Schroeder, C. L. Foiles, and D. Greig, Introduction, in *Thermoelectric Power of Metals*, edited by F. J. Blatt, P. A. Schroeder, C. L. Foiles, and D. Greig (Springer US, Boston, MA, 1976).
- [6] W. Jones and N. H. March, *Theoretical solid state physics* (Dover Publications, New York, 1985).
- [7] K. Kuroki and R. Arita, “pudding mold” Band Drives Large Thermopower in Na_xCoO_2 , *Journal of the Physical Society of Japan* **76**, 083707 (2007).
- [8] H. Usui, R. Arita, and K. Kuroki, First-principles study on the origin of large thermopower in hole-doped LaRhO_3 and CuRhO_2 , *Journal of Physics: Condensed Matter* **21**, 064223 (2009).
- [9] H. Usui, K. Kuroki, S. Nakano, K. Kudo, and M. Nohara, Pudding-Mold-Type Band as an Origin of the Large Seebeck Coefficient Coexisting with Metallic Conductivity in Carrier-Doped FeAs_2 and PtSe_2 , *Journal of Electronic Materials* **43**, 1656 (2014).
- [10] A. I. Romanenko, G. E. Chebanova, T. Chen, W. Su, and H. Wang, Review of the thermoelectric properties of layered oxides and chalcogenides, *Journal of Physics D: Applied Physics* **55**, 143001 (2022).
- [11] H. Kuriyama, M. Nohara, T. Sasagawa, K. Takubo, T. Mizokawa, K. Kimura, and H. Takagi, High-temperature thermoelectric properties of delafossite oxide $\text{CuRh}_{1-x}\text{Mg}_x\text{O}_2$, in *2006 25th International Conference on Thermoelectrics* (2006) pp. 97–98.
- [12] K. Kurita, H. Sakabayashi, and R. Okazaki, Correlation in transport coefficients of hole-doped CuRhO_2 single crystals, *Physical Review B* **99**, 115103 (2019).
- [13] J. Gu, Y. Yan, J. W. Krizan, Q. D. Gibson, Z. M. Dzwilek, R. J. Cava, and A. B. Bocarsly, p-Type CuRhO_2 as a Self-Healing Photoelectrode for Water Reduction under Visible Light, *Journal of the American Chemical Society* **136**, 830 (2014).
- [14] W. Koshibae, K. Tsutsui, and S. Maekawa, Thermopower in cobalt oxides, *Physical Review B* **62**, 6869 (2000).
- [15] P. Giannozzi, S. Baroni, N. Bonini, M. Calandra, R. Car, C. Cavazzoni, D. Ceresoli, G. L. Chiarotti, M. Cococcioni, I. Dabo, A. Dal Corso, S. de Gironcoli, S. Fabris, G. Fratesi, R. Gebauer, U. Gerstmann, C. Gougoussis, A. Kokalj, M. Lazzeri, L. Martin-Samos, N. Marzari, F. Mauri, R. Mazzarello, S. Paolini, A. Pasquarello, L. Paulatto, C. Sbraccia, S. Scandolo, G. Sclauzero, A. P. Seitsonen, A. Smogunov, P. Umari, and R. M. Wentzcovitch, QUANTUM ESPRESSO: a modular and open-

- source software project for quantum simulations of materials, *Journal of Physics: Condensed Matter* **21**, 395502 (2009).
- [16] G. Prandini, A. Marrazzo, I. E. Castelli, N. Mounet, and N. Marzari, Precision and efficiency in solid-state pseudopotential calculations, *npj Computational Materials* **4**, 1 (2018).
- [17] K. Lejaeghere, G. Bihlmayer, T. Björkman, P. Blaha, S. Blügel, V. Blum, D. Caliste, I. E. Castelli, S. J. Clark, A. Dal Corso, S. de Gironcoli, T. Deutsch, J. K. Dewhurst, I. Di Marco, C. Draxl, M. Dulak, O. Eriksson, J. A. Flores-Livas, K. F. Garrity, L. Genovese, P. Giannozzi, M. Giantomassi, S. Goedecker, X. Gonze, O. Grånäs, E. K. U. Gross, A. Gulans, F. Gygi, D. R. Hamann, P. J. Hasnip, N. A. W. Holzwarth, D. Iuşan, D. B. Jochym, F. Jollet, D. Jones, G. Kresse, K. Koepf, E. Küçükbenli, Y. O. Kvashnin, I. L. M. Locht, S. Lubeck, M. Marsman, N. Marzari, U. Nitzsche, L. Nordström, T. Ozaki, L. Paulatto, C. J. Pickard, W. Poelmans, M. I. J. Probert, K. Refson, M. Richter, G.-M. Rignanese, S. Saha, M. Scheffler, M. Schlipf, K. Schwarz, S. Sharma, F. Tavazza, P. Thunström, A. Tkatchenko, M. Torrent, D. Vanderbilt, M. J. van Setten, V. Van Speybroeck, J. M. Wills, J. R. Yates, G.-X. Zhang, and S. Cottenier, Reproducibility in density functional theory calculations of solids, *Science* **351**, aad3000 (2016).
- [18] E. Bertaut and J. Dulac, Sur l'isomorphisme d'oxydes ternaires de chrome et de rhodium trivalents, *Journal of Physics and Chemistry of Solids* **21**, 118 (1961).
- [19] G. K. Madsen and D. J. Singh, BoltzTraP. A code for calculating band-structure dependent quantities, *Computer Physics Communications* **175**, 67 (2006).
- [20] S. Hüfner, *Photoelectron spectroscopy: principles and applications* (Springer-Verlag, Berlin; New York, 1995) oCLC: 680387137.
- [21] J. P. Perdew, Density functional theory and the band gap problem, *International Journal of Quantum Chemistry* **28**, 497 (1985).
- [22] S. Shibusaki, W. Kobayashi, and I. Terasaki, Transport properties of the delafossite Rh oxide $\text{Cu}_{1-x}\text{Ag}_x\text{Rh}_{1-y}\text{Mg}_y\text{O}_2$: Effect of Mg substitution on the resistivity and Hall coefficient, *Physical Review B* **74**, 235110 (2006).